Letter

Measurement-based time evolution for quantum simulation of fermionic systems

Woo-Ram Lee,[1] Zhangjie Qin,[1] Robert Raussendorf,[2] Eran Sela,[3] and V. W. Scarola[1,*]

[1]*Department of Physics, Virginia Tech, Blacksburg, Virginia 24061, USA*

[2]*Department of Physics and Astronomy, University of British Columbia, Vancouver, BC V6T 1Z1, Canada*

[3]*Department of Physics and Astronomy, Tel Aviv University, Tel Aviv 6997801, Israel*

(Received 3 November 2021; revised 17 May 2022; accepted 31 May 2022; published 25 July 2022)

Quantum simulation using time evolution in phase-estimation-based quantum algorithms can yield unbiased solutions of classically intractable models. However, long runtimes open such algorithms to decoherence. We show how measurement-based quantum simulation uses effective time evolution via measurement to allow runtime advantages over conventional circuit-based algorithms that use real-time evolution with quantum gates. We construct a hybrid algorithm to find energy eigenvalues in fermionic models using only measurements on graph states. We apply the algorithm to the Kitaev and Hubbard chains. Resource estimates show a runtime advantage if measurements can be performed faster than gates, and graph states compactification is fully used. In this letter, we set the stage to allow advances in measurement precision to improve quantum simulation.

DOI: 10.1103/PhysRevResearch.4.L032013

I. INTRODUCTION

Unbiased quantum simulation [1,2] of intractable models aids in validating approximations. Compelling open problems include the two-dimensional Hubbard model of the cuprates and, more generally, materials and quantum chemistry models [3–17]. Such interacting fermionic models are typically NP-hard because they suffer from the fermion sign problem [18] and are generally parameterized as $H = \sum_{i,j} w_{ij} c_i^\dagger c_j + \sum_{i,j,k,l} V_{ijkl} c_i^\dagger c_j^\dagger c_k c_l$, where $c_j^\dagger$ creates a fermion in quantum state j (a composite index for spin, lattice site, etc.), and $w_{ij}(V_{ijkl})$ is the single (two)-particle Hamiltonian matrix element. Since they are NP-hard, classical simulation time increases exponentially with particle number. Unbiased quantum simulation of models captured by H will therefore offer high-impact benchmarks. Variational quantum algorithms offer promise on near-term devices [19] because they can be used to rigorously bound ground state energies.

Recent work [20] combines a variational quantum algorithm with measurement-based quantum computing (MBQC) [21,22] for efficient management of variational ansatz states. MBQC starts with a resource state, e.g., a graph state such as the square lattice cluster state (SLCS), formed by taking qubits aligned along the Pauli-x direction and then entangling them pairwise with controlled-Z gates. All quantum algorithms can then be executed using just single-qubit measurements on the resource state. MBQC-based variational algorithms [20] can therefore use measurements to bound ground state energies.

Phase-estimation-based quantum simulation algorithms [4,23–27] can go beyond variational bounds to yield exact eigenfunctions and eigenvalues of H for use in benchmarking excited state properties. In circuit-based quantum computing (CBQC), such algorithms take an input wave function $|\psi_I\rangle$ and repeatedly apply quantum gates to time-evolve H with M small time steps δt_g to eventually extract information. Quantum algorithms based on this procedure yield an advantage over classical algorithms but for runtimes that increase exponentially with the required bit precision in, e.g., eigenvalues. Long runtimes can be prohibitive [11,12,28] if, for N_g gates per time step, the qubits cannot be kept coherent for long execution times $T_C \sim MN_g\delta t_g$.

We propose revisiting phase-estimation-based quantum simulation runtime from the MBQC perspective. We consider the following regime: (i) A large number of qubits are available, (ii) the time taken for an accurate single-qubit measurement δt_m can be made small enough to avoid decoherence of the resource state, and (iii) the entangling gates are performed in parallel mostly at the beginning. Assumption (iii) allows slow/error-prone entangling gates to be implemented and error corrected in a time that is negligible compared with the time to execute all measurements.

In this letter, we explicitly map real-time evolution in CBQC (repeated application of gates that take a finite amount of time) to repeated measurement in MBQC [22]. To this end, we make the following advances: (i) We construct a route to use MBQC to effectively time-evolve H using just single-qubit measurements. We show that long effective time evolution corresponds to M sequential measurement rounds in MBQC, thus requiring coherence among non-measured qubits for a total time $T_M \sim MN_m\delta t_m$, where N_m is the number of measurements per round. (ii) We construct an example hybrid MBQC algorithm with a quantum

*scarola@vt.edu

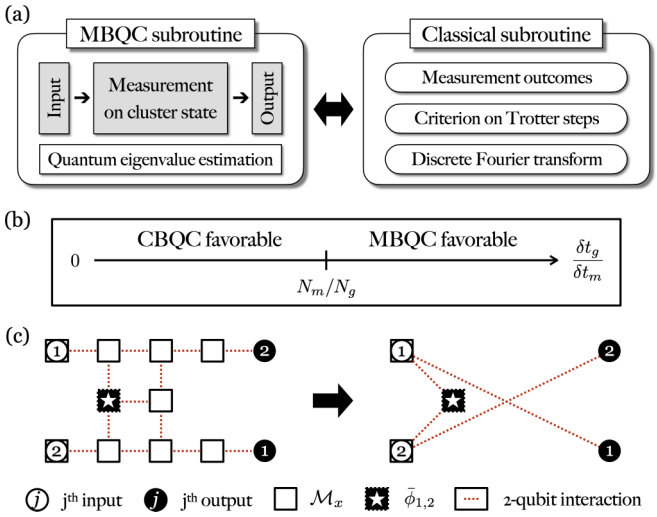

FIG. 1. (a) Schematic for the hybrid quantum eigenvalue estimation algorithm. (b) Measurement-based quantum computing (MBQC)/circuit-based quantum computing (CBQC)-favorable regimes determined by the hardware-dependent parameter $\delta t_g/\delta t_m$. The point N_m/N_g is obtained by setting the MBQC and CBQC runtimes to be the same $T_M = T_C$. (c) Measurement-based effective time evolution used for a two-site Jordan-Wigner string where information flows from left to right. Each box/circle hosts a single qubit entangled along red-dotted lines. Open (filled) circles are input (output) qubits. Open squares are Pauli-x measurements that can be performed in parallel, and the dotted box around the central star indicates an adaptive measurement with an angle dictating the time step. The left panel uses the square lattice cluster state (SLCS); the right panel is one of many equivalent graph states that can be used instead, see Supplemental Material [30].

phase-estimation-based subroutine that yields exact eigenenergies: quantum eigenvalue estimation using an offline (classical) time series [6,29]; see Fig. 1(a). (iii) We apply the algorithm to solve the Kitaev [31,32] and Hubbard [33] chains because they can be solved exactly and can therefore be accurately checked as first implementations. To compare T_M and T_C for our algorithm, we compute scaling of MBQC measurement time and precision costs as well as gate counts in an equivalent CBQC algorithm.

Our central finding is that MBQC can yield a runtime advantage over CBQC, i.e., $T_M < T_C$, by shifting the burden of requiring low δt_g but high-fidelity gates in CBQC simulation to the requirement of low δt_m and high single-qubit measurement precision in MBQC simulation. Figure 1(b) summarizes our finding by showing that, if $\delta t_g/\delta t_m$ is large, MBQC will have shorter runtimes. Here, N_m/N_g is set by the algorithm. We find that graph state compactification [34] can yield hybrid MBQC algorithms with $N_m/N_g = 1$. In this letter, therefore, we establish a route to use improvements in quantum sensing [35] to advance the state of the art in quantum simulation with effective time evolution.

II. MEASUREMENT-BASED TIME EVOLUTION

Time evolution of Hamiltonians containing noncommuting terms H_1 and H_2 requires a decomposition. The first-order Trotter-Suzuki decomposition is simplest [36,37]: $\exp[-i(H_1+H_2)t] = [\exp(-iH_1t/M)\exp(-iH_2t/M)]^M + \mathcal{O}[(t/M)^2]$. Here, the time step t/M is repeated M times until the output state is converged within a tolerance δ_T [38], and $\hbar = 1$.

To map between fermions and qubits in H, we use the Jordan-Wigner (JW) transformation [39]: $c_j^\dagger = \prod_{k=1}^{j-1}[-\sigma_z^{(k)}][\sigma_x^{(j)} + i\sigma_y^{(j)}]/2$, where σ_a with $a \in \{x, y, z\}$ are the Pauli matrices. Long JW strings containing N qubits can arise in certain models, e.g., those with long-range hopping/interaction in H. Longer-range terms allow simulation of higher-dimensional fermionic models H because they map to one-dimensional chains with long-range hopping and long-range interaction. Time evolution of a string requires the ability to execute nontrivial unitaries: $R^{(1,2\cdots N)}_{a_1a_2\cdots a_N}(\theta) = \exp[-i(\theta/2)\prod_{j=1}^N \sigma_{a_j}^{(j)}]$, where θ is a rotation angle.

The JW transformation enables construction of a time-to-angle mapping for MBQC simulation. Figure 1(c) shows an example measurement pattern needed for time evolution of a hop between neighboring sites $c_1^\dagger c_2 + c_2^\dagger c_1$. In the absence of the central measurement (star), the measurement pattern swaps information on qubits 1 and 2 [22,30]. However, the additional adaptive measurement in the second round of measurements with $\bar{\phi}_{1,2}$ on the central qubit (star) incorporates results from the first round to yield [22] $R_{zz}^{(1,2)}(\theta)|\psi_I\rangle$, where θ defines the part not relying on random measurement outcomes in $\bar{\phi}_{1,2}$. This operation is a time propagator, and one can show, see Supplemental Material [30], that, with a few more measurements, this measurement pattern effectively time-evolves a hop between sites 1 and 2.

Figure 1(c) generalizes to time evolution of longer-range terms in H on a larger SLCS using only $\mathcal{O}(1)$ adaptive measurements. Consider, e.g., a long-range hop between sites 1 and N: $c_1^\dagger c_N + c_N^\dagger c_1$. To implement effective time evolution of the JW term, we must execute the unitary $R_{zz\cdots z}^{(1,2\cdots N)}(\theta)$ (and follow up with a few rotations on the end qubits). This can be implemented with two rounds of measurements on $[(2N-1)^2 - (N-1)]$ qubits on the central area of the measurement pattern (excluding input and output qubits). The first round measures all but a central qubit, and the second round measures just the central qubit in an adaptive basis, see Supplemental Material [30], thus showing a considerable simplification in implementing long JW strings.

The number of measurements and qubits needed for effective time evolution on a SLCS, e.g., the left side of Fig. 1(c), can be significantly reduced. The Gottesman-Knill theorem [40] shows that all qubits with Pauli-x measurements can be excluded since Clifford operations can be efficiently executed classically. After mathematically removing local Pauli measurements, the SLCS maps to a compactified cluster state (CCS) [34]. The mappings show that a much smaller graph state is needed. For example, the right side of Fig. 1(c) shows an equivalent execution of $R_{zz}^{(1,2)}(\theta)$ (see Supplemental Material [30] for a proof), where the number of qubits (measurements) reduces from 12(10) to 5(3). In general, a CCS offers a reduction in measurement and qubit overhead for executing effective time evolution using $R_{zz\cdots z}^{(1,2\cdots N)}(\theta)$ by as much as $\mathcal{O}(N^2)$, depending on which CCS is chosen. We construct example time-evolution subroutines on

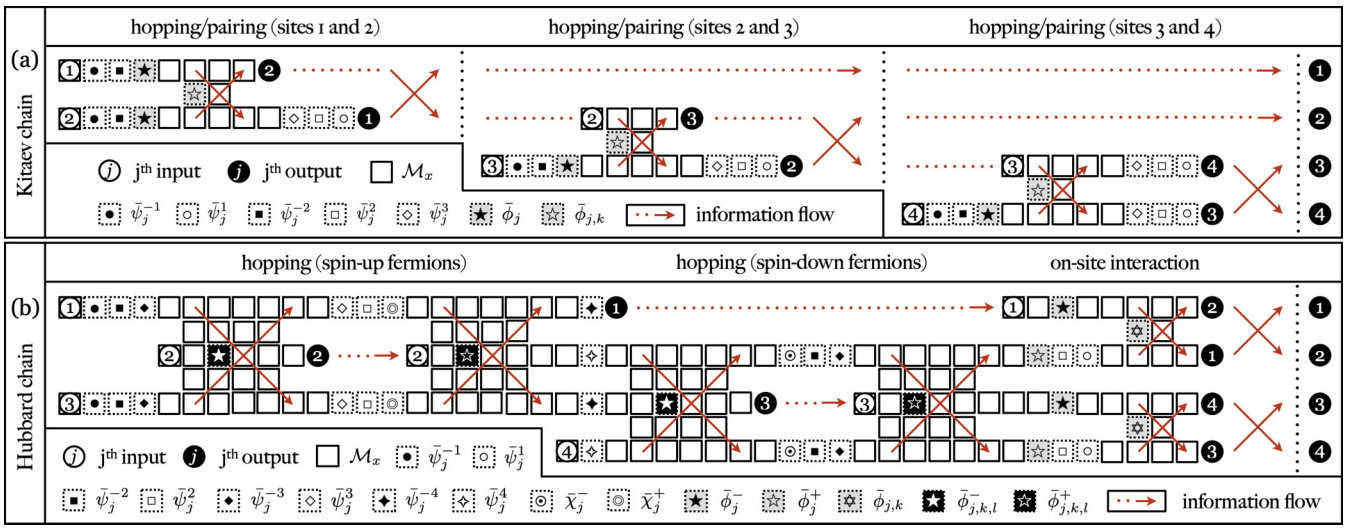

FIG. 2. (a) Subroutine for implementing $\exp(-iH_{\rm K}t)|\psi_{\rm I}\rangle$ for four sites using only measurements on a square lattice cluster state (SLCS), as in Fig. 1(c). Adaptive measurements are carried out with the angles defined in Eq. (4). The indices $j, k \in \{1, 2, 3, 4\}$ are assigned along the direction of information flow (red arrows). Measurement angles denoted by stars execute effective time evolution, while other shapes denote measurements to perform rotations at the ends of the Jordan-Wigner (JW) strings. All qubits but inputs with Pauli-x measurements (open boxes) can be removed in compactified cluster states (CCSs). (b) The same but for a two-site Hubbard chain with angles defined by Eq. (7) and $j, k, l \in \{1, 2, 3, 4\}$.

SLCSs with the understanding that use of a CCS reduces the number of required qubits and measurements at the expense of modifying qubit connectivities which is efficiently programmable [41].

III. KITAEV CHAIN

We construct an MBQC subroutine for time evolution of an example model with noncommuting terms, the Kitaev chain [31,32]:

$$H_{\rm K} = w\sum_{j=1}^{N-1}(-c_j^\dagger c_{j+1} + c_j c_{j+1} + \text{H.c.}) - \mu\sum_{j=1}^{N}\delta n_j, \quad (1)$$

where $w \geqslant 0$ is the hopping and pairing energy, $\mu \geqslant 0$ is the chemical potential, and $\delta n_j = c_j^\dagger c_j - \frac{1}{2}$. The ground state exhibits a quantum phase transition at $\mu = 2w$ between a nontopological strong-coupling phase ($\mu > 2w$) and a topological weak-coupling phase ($\mu < 2w$).

We map fermions to qubits to construct both circuit- and measurement-based time propagators. The JW transformation maps $H_{\rm K}$ to the quantum Ising model. The first-order Trotterized form of $\exp(-iH_{\rm K}t)$ is

$$\left[\prod_{j,k} R_{xx}^{(j,j+1)}(-2\phi_M)R_z^{(k)}(-2g_\mu\phi_M)\right]^M, \quad (2)$$

where $g_\mu = \mu/(2w)$, and

$$\phi_M = \frac{wt}{M} \quad (3)$$

is a measurement angle. Equation (2) can be implemented in two different ways: using real-time evolution in CBQC or effective time evolution in MBQC, where M dictates the circuit or measurement depth, respectively. Equation (3) is central because it maps real time t to measurement angle.

We use the stabilizer formalism to map Eq. (2) to effective time evolution in MBQC. Figure 2(a) shows the measurement pattern implementing Eq. (2) to time-evolve input qubits 1–4 (open circles) with just single-qubit measurements. The measurement angles in the x-y plane are

$$\bar\phi_{j,k} = 2P_{\bar\phi_{j,k}}\phi_M, \quad \bar\phi_j = -P_{\bar\phi_j}(2g_\mu\phi_M + \gamma),$$
$$\bar\psi_j^r = P_{\bar\psi_j^r}\psi^r, \quad (4)$$

where $\psi^r \in \{\pm\alpha, \pm\beta, \gamma\}$ for $r = \pm1, \pm2, 3$, $-\alpha = \beta = \gamma = \pi/2$, and $P_\theta = (-1)^{S_\theta^{\rm K}}$. Here, $S_\theta^{\rm K}$ accumulates all measurement outcomes during single-qubit measurements and is derived in the Supplemental Material [30]. The measurement outcomes are also used for offline processing with a byproduct operator, see Supplemental Material [30], that defines the basis for interpreting output measurements.

The left, middle, and right panels depict measurements [stars in Fig. 2(a)] that entangle input qubits 1-2, 2-3, and 3-4, respectively. The measurement pattern in Fig. 2(a) and Eq. (4) define the full effective time-evolution algorithm for a Kitaev chain of any N or M because additional panels in Fig. 2(a) can be concatenated, see Supplemental Material [30]. The red dots and arrows show information flow for use in concatenation.

IV. HUBBARD CHAIN

We now turn to the Hubbard chain [33] with a longer JW string and an important interaction term:

$$H_{\rm H} = -w\sum_{j=1,\sigma}^{N-1}(c_{j,\sigma}^\dagger c_{j+1,\sigma} + \text{H.c.}) + U\sum_{j=1}^{N} n_{j,\uparrow}n_{j,\downarrow}, \quad (5)$$

where $\sigma \in \{\uparrow, \downarrow\}$, U is the Hubbard interaction strength, and $n_{j,\sigma} = c^\dagger_{j,\sigma} c_{j,\sigma}$. To map fermions to qubits, we introduce [42] spinless fermion operators: $\tilde{c}_{2j-1} = c_{j,\uparrow}$ and $\tilde{c}_{2j} = c_{j,\downarrow}$. The JW mapping then leads to an equivalent qubit Hamiltonian: $(w/2)\sum_{j=1}^{2N-2}[\sigma_x^{(j)}\sigma_z^{(j+1)}\sigma_x^{(j+2)} + \sigma_y^{(j)}\sigma_z^{(j+1)}\sigma_y^{(j+2)}] + (U/4)\sum_{j=1}^{N}[\mathbb{I}_{2j-1} + \sigma_z^{(2j-1)}][\mathbb{I}_{2j} + \sigma_z^{(2j)}]$, where the JW strings used for the hopping terms need a three-qubit entangling gate, and $\mathbb{I} = \mathrm{diag}(1, 1)$. The first-order Trotterized form of $\exp(-iH_{\mathrm{H}}t)$ is

$$\left[\prod_{j,k} R_{zz}^{(2j-1,2j)}(g_U\phi_M) R_z^{(2j-1)}(g_U\phi_M) R_z^{(2j)}(g_U\phi_M) \times R_{xzx}^{(k,k+1,k+2)}(\phi_M) R_{yzy}^{(k,k+1,k+2)}(\phi_M)\right]^M, \tag{6}$$

where $g_U = U/(2w)$.

Equation (6) can be used in CBQC or mapped to single-qubit measurements in MBQC. Figure 2(b) depicts the $N = 2$ measurement pattern for Eq. (6) with measurement angles:

$$\begin{aligned} &\bar{\phi}^{\pm}_{j,k,l} = -P_{\bar{\phi}^{\pm}_{j,k,l}}\phi_M, \quad \bar{\phi}_{j,k} = -P_{\bar{\phi}_{j,k}} g_U \phi_M, \\ &\bar{\psi}^r_j = P_{\bar{\psi}^r_j}\psi^r, \quad \bar{\phi}^{\pm}_j = \pm P_{\bar{\phi}^{\pm}_j}\left[g_U\phi_M + \frac{(1\pm 1)\gamma}{2}\right], \\ &\bar{\chi}^{\pm}_j = \pm P_{\bar{\chi}^{\pm}_j}(\lambda + \alpha), \end{aligned} \tag{7}$$

where $\psi^r \in \{\pm\alpha, \pm\beta, \pm\gamma, \pm\lambda\}$ for $r = \pm 1, \pm 2, \pm 3, \pm 4$, $\lambda = \alpha$, and $P_\theta = (-1)^{S^{\mathrm{H}}_\theta}$. Here, S^{H}_θ is derived in the Supplemental Material [30]. The Hubbard chain measurement pattern can also be concatenated to time-evolve larger N or M, see Supplemental Material [30], and overhead can be significantly reduced in a CCS.

Both examples, Eq. (4) for H_{K} and Eq. (7) for H_{H}, demonstrate constraints on effective time evolution. Long effective time evolution from a larger number of Trotter steps in MBQC corresponds to smaller measurement angles since $\phi_M \propto 1/M$. Repeated small-angle measurements (long effective time evolution) in MBQC therefore require improvements in qubit measurement precision as opposed to faster gates in CBQC.

V. EIGENVALUE ESTIMATION

To demonstrate resource requirements, we construct a minimal hybrid quantum eigenvalue estimation algorithm by combining MBQC subroutines with an offline time-series estimator [Fig. 1(a)]. A $|\psi_{\mathrm{I}}\rangle$ close to a desired eigenstate is fed into the MBQC time-evolving subroutine yielding $\langle\psi_{\mathrm{I}}|e^{-iHt}|\psi_{\mathrm{I}}\rangle$ if the output qubits are measured using quantum state tomography (or an ancilla qubit [6]) to find the wave function phase relative to the input qubit basis. The MBQC output is obtained L times and used in a classical discrete Fourier transform:

$$\mathcal{A}(\omega_m) = \frac{\delta t}{\pi}\sum_{n=0}^{L-1}\mathrm{Re}\{\exp[(i\omega_m - \eta)t_n]\langle\psi_{\mathrm{I}}|\exp(-iHt_n)|\psi_{\mathrm{I}}\rangle\}, \tag{8}$$

where we define $t_n = n\delta t$, $\omega_m = m\delta\omega$ ($n, m = 0, 1, \cdots, L-1$) in units of δt and $\delta\omega$ satisfying $\delta\omega\delta t = 2\pi/L$. Peaks in $\mathcal{A}(\omega)$ yield eigenvalues of H to within δ_{T}. We introduce the broadening parameter $\eta > 0$ for visualization of Lorentzian peaks and as a proxy for experimentally limited resolution.

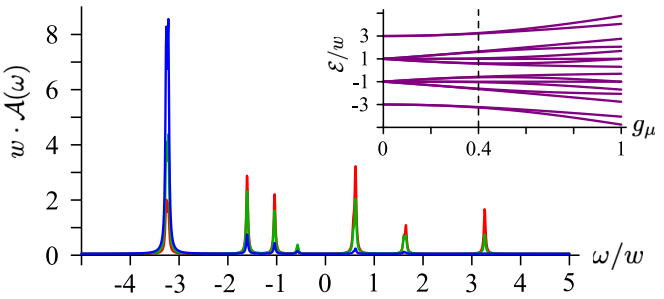

FIG. 3. Main: Simulation using Eq. (8), where peaks reveal the exact eigenenergies of the four-site Kitaev chain with $g_\mu = 0.4$, $\eta/w = 0.02$, and $\delta\omega/w = 0.01$. Trotter error is $\delta_{\mathrm{T}} = 10^{-2}$ for $M < 8500$, and $L = 1272$ is chosen for clarity. $|\psi_{\mathrm{I}}\rangle$ is chosen to be the ground state at $g_\mu = 0$. The blue line indicates the error-free case, and the green and red lines plot the impact of random perturbations [45–56% (green); 70–82% (red)] in the measurement angles $\bar{\phi}_j$ and $\bar{\psi}^3_j$. Inset: Eigenenergies of Eq. (1), where the energies touching the dashed line match the peak positions in the main panel.

The main panel in Fig. 3 shows a demonstration result from a simulation using H_{K} in Eq. (8), where several eigenvalues are returned as peaks. One can show, see Supplemental Material [30], that peak centers are intact while peak weights are shifted for certain types of measurement errors. Figure 3 uses large L and M for clarity, but in practice, L and M can be lowered. They are minimized by restricting the search to just the ground state energy, while three independent algorithm input parameters $\delta\omega$, L, and M must be chosen to meet three tolerances: (i) $\delta\omega$ should be smaller than η to resolve peak structure, (ii) a sum rule tolerance $\delta_{\mathrm{F}} > |1 - \delta\omega\sum_{m=0}^{L-1}\mathcal{A}(\omega_m)|$ sets L, and (iii) M is set by requiring δ_{T} to be much smaller than the first spectral gap.

VI. MEASUREMENT PRECISION

The number of Trotter steps yields the measurement depth and sets ϕ_M. Large M improves Trotter accuracy at the expense of requiring improved measurement precision (small ϕ_M). To estimate the minimum M needed to obtain ground state energies, we consider H_{K} with $g_\mu = 0.01$–0.4. We find empirically, see Supplemental Material [30], that, for each n in Eq. (8), the minimum M varies from 1.8×10^3 ($g_\mu = 0.01$) to 7.8×10^4 ($g_\mu = 0.4$) to resolve the ground state energy of H_{K} to within 1% of the spectral gap ($\delta_{\mathrm{T}} = 10^{-2}$) for $\eta = 0.02w$, $\delta\omega = 0.01w$, $L = 46$, and $N = 4$. We have checked $N \leqslant 8$ with other $\eta, \delta\omega$, and L combinations and obtained similar results for M. In general, the M needed will depend on the model, model parameters, tolerances, and scales as $\mathcal{O}[(Nt_n)^2\delta_{\mathrm{T}}^{-1}]$ [43], thus implying that the required measurement depth and precision to execute effective MBQC time evolution can become demanding [44].

Given bounds on M, we can estimate measurement precision requirements for H_{K}. Here, ϕ_M depends on n. The largest measurement angle (in units of 2π) needed to implement Eq. (8) with Eq. (4) is χ_{L-1}, where $\chi_n \equiv nw/(\delta\omega LM)$. We

TABLE I. Resources for a single time step in Eq. (8) computed by counting and concatenation, see Supplemental Material [30], in three scenarios(rows): (i) MBQC on an SLCS including all Pauli-x and adaptive measurements, (ii) MBQC on a CCS with the least number of measurements, and (iii) CBQC. In (i) and (ii), measurements on input/output qubits are not counted. (ii) and (iii) show the same scaling ($N_m/N_g = 1$) for two different experimental processes, measurements and two-qubit gates.

Approach	H_{K}	H_{H}
SLCS measurements, N_m	$(17N-10)M$	$(156N-144)M$
CCS measurements, N_m	$(7N-1)M$	$(34N-32)M$
Circuit-based gates, N_g	$(7N-1)M$	$(34N-32)M$

empirically find, see Supplemental Material [30] (far from the critical point at $g_\mu = 1$), $\chi_n \lesssim 0.14$, thus allowing the use of Eq. (3). The smallest measurement angle increment needed in Eq. (4) is $g_\mu \chi_n$. We find $g_\mu \chi_n \gtrsim 4.8 \times 10^{-4}$ for all $g_\mu < 1$ and n. We therefore see that a large M requires small angle measurements as we implement effective time evolution.

VII. MEASUREMENT AND QUBIT OVERHEAD

The measurement subroutines defined by Eqs. (4) and (7) allow estimates of resource requirements in our hybrid quantum eigenvalue estimation algorithm. Table I shows, see Supplemental Material [30], that, for the local models considered here, a CCS will have $N_m/N_g = 1$. However, with nonlocal qubit terms, e.g., for nonlocal hopping in H, MBQC with a CCS will have an $\mathcal{O}(N)$ advantage in measurement vs gate counts in CBQC unless nonlocal gates are used to implement the JW strings [45]. The number of qubits needed is $\mathcal{O}(M)$ larger for MBQC than for CBQC. MBQC qubit overhead can be lowered by re-entangling measured qubits [21].

VIII. DISCUSSION

Our demonstration algorithms show that unbiased quantum simulation using effective time evolution is possible using only single-qubit measurements on graph states. We find that long MBQC effective time evolution for use in quantum simulation requires high measurement precision to be useful in benchmarking approximate classical algorithms. Alternative time-evolution decompositions [16,46–49] will lower overhead.

MBQC offers advantages in systems with slow/error-prone entangling gates [50], e.g., photonics [51,52] and atoms in optical lattices [21]. In the latter case, parallelized collisional gates encoded large SLCSs in long-lived atomic hyperfine states [53]. Recent progress in single-site measurements [54] and control [55] allow optical lattice implementation of MBQC effective time-evolution algorithms.

The above algorithms have a low error threshold [56,57]. An improvement with higher thresholds is available [58,59]. The above algorithms can also be used in conjunction with an adaptive Bayesian algorithm (instead of a time series) in eigenvalue estimation learning certain types of error [60,61].

Finally, applications to higher-dimensional fermionic models are highly desired. Nearest neighbor hoppings/interactions in a higher-dimensional fermionic lattice can be mapped to long-range hoppings/interactions in a chain [6]. After mapping, our hybrid MBQC algorithm can be applied to the chain at the expense of increasing the length of JW strings.

ACKNOWLEDGMENTS

We acknowledge support from ARO (W911NF2010013). W.-R.L., Z.Q., and V.W.S. acknowledge support from AFOSR (FA9550-18-1-0505, FA9550-19-1-0272).

[1] R. P. Feynman, Simulating physics with computers, Int. J. Theor. Phys. **21**, 467 (1982).
[2] I. M. Georgescu, S. Ashhab, and F. Nori, Quantum simulation, Rev. Mod. Phys. **86**, 153 (2014).
[3] D. S. Abrams and S. Lloyd, Simulation of Many-Body Fermi Systems on a Universal Quantum Computer, Phys. Rev. Lett. **79**, 2586 (1997).
[4] D. S. Abrams and S. Lloyd, Quantum Algorithm Providing Exponential Speed Increase for Finding Eigenvalues and Eigenvectors, Phys. Rev. Lett. **83**, 5162 (1999).
[5] G. Ortiz, J. E. Gubernatis, E. Knill, and R. Laflamme, Quantum algorithms for fermionic simulations, Phys. Rev. A **64**, 022319 (2001).
[6] R. Somma, G. Ortiz, J. E. Gubernatis, E. Knill, and R. Laflamme, Simulating physical phenomena by quantum networks, Phys. Rev. A **65**, 042323 (2002).
[7] A. Aspuru-Guzik, Simulated quantum computation of molecular energies, Science **309**, 1704 (2005).
[8] I. Kassal, J. D. Whitfield, A. Perdomo-Ortiz, M.-H. Yung, and A. Aspuru-Guzik, Simulating chemistry using quantum computers, Annu. Rev. Phys. Chem. **62**, 185 (2011).
[9] M.-H. Yung, J. D. Whitfield, S. Boixo, D. G. Tempel, and A. Aspuru-Guzik, Introduction to quantum algorithms for physics and chemistry, in *Quantum Information and Computation for Chemistry*, edited by S. A. Rice, A. R. Dinner, and S. Kais (John Wiley and Sons, Inc., Hoboken, 2014), Vol. 154, pp. 67–106.
[10] D. Wecker, B. Bauer, B. K. Clark, M. B. Hastings, and M. Troyer, Gate-count estimates for performing quantum chemistry on small quantum computers, Phys. Rev. A **90**, 022305 (2014).
[11] J. R. McClean, R. Babbush, P. J. Love, and A. Aspuru-Guzik, Exploiting locality in quantum computation for quantum chemistry, J. Phys. Chem. Lett. **5**, 4368 (2014).
[12] D. Wecker, M. B. Hastings, N. Wiebe, B. K. Clark, C. Nayak, and M. Troyer, Solving strongly correlated electron models on a quantum computer, Phys. Rev. A **92**, 062318 (2015).
[13] B. Bauer, D. Wecker, A. J. Millis, M. B. Hastings, and M. Troyer, Hybrid Quantum-Classical Approach to Correlated Materials, Phys. Rev. X **6**, 031045 (2016).
[14] J. R. McClean, M. E. Kimchi-Schwartz, J. Carter, and W. A. de Jong, Hybrid quantum-classical hierarchy for mitigation of

decoherence and determination of excited states, Phys. Rev. A **95**, 042308 (2017).
[15] R. Babbush, N. Wiebe, J. McClean, J. McClain, H. Neven, and G. K.-L. Chan, Low-Depth Quantum Simulation of Materials, Phys. Rev. X **8**, 011044 (2018).
[16] D. Poulin, A. Kitaev, D. S. Steiger, M. B. Hastings, and M. Troyer, Quantum Algorithm for Spectral Measurement with a Lower Gate Count, Phys. Rev. Lett. **121**, 010501 (2018).
[17] S. McArdle, S. Endo, A. Aspuru-Guzik, S. C. Benjamin, and X. Yuan, Quantum computational chemistry, Rev. Mod. Phys. **92**, 015003 (2020).
[18] M. Troyer and U.-J. Wiese, Computational Complexity and Fundamental Limitations to Fermionic Quantum Monte Carlo Simulations, Phys. Rev. Lett. **94**, 170201 (2005).
[19] N. Moll, P. Barkoutsos, L. S. Bishop, J. M. Chow, A. Cross, D. J. Egger, S. Filipp, A. Fuhrer, J. M. Gambetta, M. Ganzhorn, A. Kandala, A. Mezzacapo, P. Müller, W. Riess, G. Salis, J. Smolin, I. Tavernelli, and K. Temme, Quantum optimization using variational algorithms on near-term quantum devices, Quantum Sci. Technol. **3**, 030503 (2018).
[20] R. R. Ferguson, L. Dellantonio, A. A. Balushi, K. Jansen, W. Dür, and C. A. Muschik, Measurement-Based Variational Quantum Eigensolver, Phys. Rev. Lett. **126**, 220501 (2021).
[21] R. Raussendorf and H. J. Briegel, A One-Way Quantum Computer, Phys. Rev. Lett. **86**, 5188 (2001).
[22] R. Raussendorf, D. E. Browne, and H. J. Briegel, Measurement-based quantum computation on cluster states, Phys. Rev. A **68**, 022312 (2003).
[23] A. Yu. Kitaev, Quantum measurements and the Abelian stabilizer problem, arXiv:quant-ph/9511026 (1995).
[24] S. Lloyd, Universal quantum simulators, Science **273**, 1073 (1996).
[25] D. W. Berry and H. M. Wiseman, Optimal States and Almost Optimal Adaptive Measurements for Quantum Interferometry, Phys. Rev. Lett. **85**, 5098 (2000).
[26] B. L. Higgins, D. W. Berry, S. D. Bartlett, H. M. Wiseman, and G. J. Pryde, Entanglement-free Heisenberg-limited phase estimation, Nature (London) **450**, 393 (2007).
[27] K. M. Svore, M. B. Hastings, and M. Freedman, Faster phase estimation, Quantum Inf. Comput. **14**, 306 (2014).
[28] A. Peruzzo, J. McClean, P. Shadbolt, M.-H. Yung, X.-Q. Zhou, P. J. Love, A. Aspuru-Guzik, and J. L. O'Brien, A variational eigenvalue solver on a photonic quantum processor, Nat. Commun. **5**, 4213 (2014).
[29] R. D. Somma, Quantum eigenvalue estimation via time series analysis, New J. Phys. **21**, 123025 (2019).
[30] See Supplemental Material at http://link.aps.org/supplemental/10.1103/PhysRevResearch.4.L032013 for the detailed proof of the main results.
[31] A. Yu. Kitaev, Unpaired Majorana fermions in quantum wires, Phys. Usp. **44**, 131 (2001).
[32] A. Kitaev and C. Laumann, Topological phases and quantum computation, in *Exact Methods in Low-Dimensional Statistical Physics and Quantum Computing*, edited by J. Jacobsen, S. Ouvry, V. Pasquier, D. Serban, and L. Cugliandolo, Lecture Notes of the Les Houches Summer School (Oxford University Press, Oxford, 2008), Vol. 89, pp. 101–125.
[33] F. H. L. Essler, H. Frahm, F. Göhmann, A. Klümper, and V. E. Korepin, *The One-Dimensional Hubbard Model* (Cambridge University Press, Cambridge, 2005), p. 302.
[34] M. Hein, J. Eisert, and H. J. Briegel, Multiparty entanglement in graph states, Phys. Rev. A **69**, 062311 (2004).
[35] C. L. Degen, F. Reinhard, and P. Cappellaro, Quantum sensing, Rev. Mod. Phys. **89**, 035002 (2017).
[36] H. F. Trotter, On the product of semi-groups of operators, Proc. Am. Math. Soc. **10**, 545 (1959).
[37] M. Suzuki, Improved Trotter-like formula, Phys. Lett. A **180**, 232 (1993).
[38] Specifically, we have $||\exp[-i(H_1+H_2)t]-[\exp(-iH_1t/M)\exp(-iH_2t/M)]^M|| < \delta_{\mathrm{T}}$, where $||A||$ is the spectral norm, i.e., the largest singular value of A.
[39] P. Jordan and E. Wigner, Über das paulische äquivalenzverbot, Z. Phys. **47**, 631 (1928).
[40] D. Gottesman, The Heisenberg representation of quantum computers, in *Proceedings of the XXII International Colloquium on Group Theoretical Methods in Physics*, edited by S. P. Corney, R. Delbourgo, and P. D. Jarvis (International Press, Cambridge, MA, 1999), pp. 32–43.
[41] S. Anders and H. J. Briegel, Fast simulation of stabilizer circuits using a graph-state representation, Phys. Rev. A **73**, 022334 (2006).
[42] W. J. Camp, Note on the one-dimensional Hubbard model, Phys. Rev. B **10**, 2903 (1974).
[43] A. M. Childs, Y. Su, M. C. Tran, N. Wiebe, and S. Zhu, Theory of Trotter Error with Commutator Scaling, Phys. Rev. X **11**, 011020 (2021).
[44] Here, δ_{T} is a strict upper bound on Trotter error, and estimates of energies with lower M are possible. Furthermore, M will decrease substantially for higher-order Trotter-Suzuki decompositions: $M \sim \mathcal{O}[(Nt_n)^{1+1/p}\delta_{\mathrm{T}}^{-1/p}]$ for the order of p.
[45] M. B. Hastings, D. Wecker, B. Bauer, and M. Troyer, Improving quantum algorithms for quantum chemistry, Quantum Inf. Comput. **15**, 1 (2015).
[46] D. W. Berry, A. M. Childs, R. Cleve, R. Kothari, and R. D. Somma, Exponential improvement in precision for simulating sparse Hamiltonians, in *Proceedings of the Forty-Sixth Annual ACM Symposium on Theory of Computing* (ACM, New York, 2014), pp. 283–292.
[47] D. Berry and L. Novo, Corrected quantum walk for optimal Hamiltonian simulation, Quantum Inf. Comput. **16**, 1295 (2016).
[48] A. M. Childs, A. Ostrander, and Y. Su, Faster quantum simulation by randomization, Quantum **3**, 182 (2019).
[49] G. H. Low and I. L. Chuang, Optimal Hamiltonian Simulation by Quantum Signal Processing, Phys. Rev. Lett. **118**, 010501 (2017).
[50] H. J. Briegel, D. E. Browne, W. Dür, R. Raussendorf, and M. Van den Nest, Measurement-based quantum computation, Nat. Phys. **5**, 19 (2009).
[51] P. Kok, W. J. Munro, K. Nemoto, T. C. Ralph, J. P. Dowling, and G. J. Milburn, Linear optical quantum computing with photonic qubits, Rev. Mod. Phys. **79**, 135 (2007).
[52] A. Pick, E. S. Matekole, Z. Aqua, G. Guendelman, O. Firstenberg, J. P. Dowling, and B. Dayan, Boosting Photonic Quantum Computation with Moderate Nonlinearity, Phys. Rev. Appl. **15**, 054054 (2021).
[53] O. Mandel, M. Greiner, A. Widera, T. Rom, T. W. Hänsch, and I. Bloch, Controlled collisions for multi-particle entanglement of optically trapped atoms, Nature (London) **425**, 937 (2003).

[54] Y. Wang, X. Zhang, T. A. Corcovilos, A. Kumar, and D. S. Weiss, Coherent Addressing of Individual Neutral Atoms in a 3D Optical Lattice, Phys. Rev. Lett. **115**, 043003 (2015).

[55] Y. Wang, A. Kumar, T.-Y. Wu, and D. S. Weiss, Single-qubit gates based on targeted phase shifts in a 3D neutral atom array, Science **352**, 1562 (2016).

[56] P. Aliferis and D. W. Leung, Simple proof of fault tolerance in the graph-state model, Phys. Rev. A **73**, 032308 (2006).

[57] C. M. Dawson, H. L. Haselgrove, and M. A. Nielsen, Noise Thresholds for Optical Quantum Computers, Phys. Rev. Lett. **96**, 020501 (2006).

[58] R. Raussendorf, J. Harrington, and K. Goyal, A fault-tolerant one-way quantum computer, Ann. Phys. **321**, 2242 (2006).

[59] R. Raussendorf and J. Harrington, Fault-Tolerant Quantum Computation with High Threshold in Two Dimensions, Phys. Rev. Lett. **98**, 190504 (2007).

[60] N. Wiebe and C. Granade, Efficient Bayesian Phase Estimation, Phys. Rev. Lett. **117**, 010503 (2016).

[61] T. E. O'Brien, B. Tarasinski, and B. M. Terhal, Quantum phase estimation of multiple eigenvalues for small-scale (noisy) experiments, New J. Phys. **21**, 023022 (2019).